

Diverse organic carbon dynamics captured by radiocarbon analysis of distinct compound classes in a grassland soil

Katherine E. Grant^{1*}, Marisa N. Repasch^{1,2,3}, Kari M. Finstad¹, Julia D. Kerr¹, Maxwell Marple¹, Christopher J. Larson^{1,4}, Taylor A. B. Broek^{1,5}, Jennifer Pett-Ridge^{1,6}, and Karis J. McFarlane¹

¹Physical and Life Sciences Directorate, Lawrence Livermore National Laboratory, Livermore, CA 94550, USA

²Institute of Arctic and Alpine Research, University of Colorado, Boulder, CO, USA

³Earth and Planetary Sciences, University of New Mexico, Albuquerque, NM, USA

⁴Department of Earth and Environmental Science, University of Pennsylvania, Philadelphia, PA, USA

⁵National Ocean Sciences Accelerator Mass Spectrometry (NOSAMS) Facility, Woods Hole Oceanographic Institution Woods Hole, MA, USA

⁶Life and Environmental Sciences Department, University of California-Merced, Merced, CA, USA

Correspondence to: Katherine E. Grant (grant39@llnl.gov)

Abstract. Soil organic carbon (SOC) is a large, dynamic reservoir composed of a complex mixture of plant and microbe derived compounds with a wide distribution of cycling timescales and mechanisms. The distinct residence times of individual carbon components within this reservoir depend on a combination of factors, including compound reactivity, mineral association, and climate conditions. To better constrain SOC dynamics, bulk radiocarbon measurements are commonly used to trace biosphere inputs into soils and estimate timescales of SOC cycling. However, understanding the mechanisms driving the persistence of organic compounds in bulk soil requires analyses of SOC pools that can be linked to plant sources and microbial transformation processes. Here, we adapt approaches, previously developed for marine sediments, to isolate organic compound classes from soils for radiocarbon (¹⁴C) analysis. We apply these methods to a soil profile from an annual grassland in Hopland, California (USA) to assess changes in SOC persistence with depth to 1 m. We measured the radiocarbon values of water extractable organic carbon (WEOC), total lipid extracts (TLE), total hydrolysable amino acids (AA), and an acid-insoluble (AI) fraction from bulk and physically separated size fractions (<2 mm, 2 mm–63 μm, and <63 μm). Our results show that Δ¹⁴C values of bulk soil, size fractions, and extracted compound classes became more depleted with depth, and individual SOC components have distinct age-depth distributions that suggest distinguishable cycling rates. We found that AA and TLE cycle faster than the bulk soils and the AI fraction. The AI was the most ¹⁴C depleted fraction, indicating it is the most chemically inert in this soil. Our approach enables the isolation and measurement of SOC fractions that separate functionally distinct SOC pools that can cycle relatively quickly (e.g., plant and microbial residues) from more passive or inert SOC pools (associated with minerals or petrogenic) from bulk soils and soil physical fractions. With the effort to move beyond SOC bulk analysis, we find that compound class ¹⁴C analysis can improve our understanding of SOC cycling and disentangle the physical and chemical factors driving OC cycling rates and persistence.

34 **1 Introduction**

35 Soil organic carbon (SOC) is a large and complex terrestrial reservoir of Earth's organic carbon (OC) (Jobbágy and
36 Jackson, 2000). It is a highly dynamic and open pool with inputs from decaying plant material, living roots, and soil microbes,
37 and with losses driven by microbial activity that includes the degradation and transformation of compounds (Angst et al.,
38 2021). The result of these processes is a heterogenous mixture of organic compounds with different radiocarbon (^{14}C) ages
39 and reactivities (Lehmann and Kleber, 2015; Shi et al., 2020; Trumbore and Harden, 1997; Gaudinski et al., 2000; McFarlane
40 et al., 2013). This complexity obscures the mechanisms that control overall OC persistence in soils, resulting in a continued
41 debate over the degree to which environmental factors, physical protection, and chemical composition influence SOC reactivity
42 and persistence (Lützow et al., 2006; Lehmann et al., 2020; Schmidt et al., 2011).

43 Bulk analysis methods do not satisfactorily demonstrate how physical protection and chemical composition interact to
44 influence SOC persistence, and so novel organic matter characterization methods can shed light on how different compound
45 classes of OC are preserved in soils and through what mechanisms. For example, we need to understand how the chemical
46 structure of OC influences interactions with mineral surfaces, such as aggregation or sorption, as well as how the environment
47 influences the decomposition and resource availability of certain OC compounds and functional groups (Lehmann and Kleber,
48 2015; Schmidt et al. 2011; Kleber et al., 2021). However, it has been difficult to isolate, identify, and quantify pools of OC
49 that directly link to in-situ OC chemical compounds (Von Lutzow et al., 2007). Thus, specific organic compounds isolated
50 from soils, such as amino acids and lipids (Rethemeyer et al., 2004), can provide information on how OC is stabilized in
51 different environments. Therefore, multiple approaches are needed to fully understand the interplay between chemical
52 compound reactivity and how carbon-mineral interaction functions as part of SOC persistence in soil.

53 One approach used to investigate the controls on SOC persistence is to separate soil into operationally defined carbon
54 pools (e.g., size or density fractions) and characterize the resulting fractions. This approach has demonstrated that association
55 of OC with soil minerals is a critical mechanism for C stabilization (Vogel et al., 2014; Mikutta et al., 2007), as ^{14}C data
56 indicate that some mineral-associated C can persist for thousands of years (Torn et al., 2009). However, ^{13}C labelling
57 experiments show that some mineral-associated C cycles quickly, within months to years (Keiluweit et al., 2015; De Troyer
58 et al., 2011). Some biomolecules form strong associations with mineral surfaces, such as long-chain lipids with iron oxides
59 (Grant et al., 2022), while other compounds only loosely associate with minerals such as through hydrophobic interactions
60 with other OC compounds (Kleber et al., 2007). Therefore, physically isolated mineral-associated OC is still a heterogenous
61 mixture of OC molecules that have a distribution of turnover times, rather than a single homogenous and intrinsically stable
62 SOC pool (Stoner et al., 2023; Van Der Voort et al., 2017).

63 Another approach that can yield finer resolution of OC turnover than traditional techniques is to isolate and measure the
64 isotopic signature of specific compounds (Von Lutzow et al., 2007). In marine, riverine, and lacustrine systems, compound
65 specific radiocarbon analysis (CSRA) has been used monitor the degradation of organic carbon through the marine water

66 column (Loh et al., 2004), characterize marine particulate OC (Hwang and Druffel, 2003), constrain terrestrial OC burial and
67 export from river systems (Galy et al., 2015; Galy et al., 2008; Repasch et al., 2021, Smittenberg et al., 2004), and determine
68 effect of OC export and burial on precipitation patterns and climate (Hein et al., 2020; Eglinton et al., 2021). Different types
69 of compounds including plant or microbial lipid biomarkers (Douglas et al., 2018; Huang et al., 1996), amino acids (Bour et
70 al., 2016; Blattmann et al., 2020), lignin (Feng et al., 2017; Feng et al., 2013), certain carbohydrate compounds (Kuzyakov et
71 al., 2014; Gleixner, 2013), and pyrogenic or black carbon (Coppola et al., 2018) can be isolated and analysed for ^{14}C leading
72 to a more detailed understanding of the cycling of targeted compounds in the environment.

73 Each of these specific compounds can provide information related to the persistence, source, and potential fate of OC in
74 soils. For instance, lipids are found in plant cell walls and microbial cell membranes and are used for energy storage. Amino
75 acids are necessary for protein formation, are enriched in nitrogen relative to other plant and microbial residues, and likely
76 play an important role in nitrogen mining and recycling. These two compound classes have diverse chemical reactivities which
77 allows for insight into chemical compound persistence. Understanding the abundance and age of these two biomarkers in soils
78 can help differentiate the source of C used by soil microbes for metabolism and growth (e.g., new C inputs vs older, recycled
79 soil C) as well as the transformation pathways that yield persistent SOC.

80 Recently, CSRA approaches developed for these environments have been applied to soil showing promise for identifying
81 distinct ages of plant and microbial biomarkers in SOC (Gies et al., 2021; Grant et al., 2022; Van Der Voort et al., 2017; Jia
82 et al., 2023; Douglas et al., 2018). Most of these CSRA studies applied to SOC have targeted specific, individual biomarkers
83 in soils, which generally contribute less than 5% of the entire carbon pool (Lützow et al., 2006; Kögel-Knabner, 2002). This
84 approach can be too specific to elucidate holistic mechanisms for SOC persistence and turnover that pertain to the majority of
85 SOC. While individual biomarker ages, such as single ages of a particular lipid or single amino acid, can be useful in some
86 contexts, comprehensive understanding of carbon compound class persistence is vital for understanding and modelling the
87 vulnerability of soil carbon to degradation.

88 To strike a balance between too specific and too broad, some researchers have characterized broader compound classes
89 rather than isolating a single biomarker. For example, this ^{14}C -compound class approach has been applied to marine dissolved
90 and particulate OC with a range of compounds, such as total lipids and total amino acids, to provide a broader understanding
91 of OC persistence in oceans (Wang et al., 2006; Wang et al., 1998; Loh et al., 2004). Wang et al. (1998) established a sequential
92 extraction procedure to analyse ^{14}C abundance of total lipids, amino acids, carbohydrates, and a residual acid insoluble fraction
93 from marine POC and sediments. This approach yielded distinct differences in ^{14}C age and abundance of the amino acids,
94 lipids, and the acid insoluble fraction in POC from the marine water column and sediment, as well as in coastal versus open
95 ocean environments. Loh et al. (2004) found the lipid fraction of dissolved OC and POC to be the oldest fraction measured in
96 both the Atlantic and Pacific oceans, while the acid insoluble fraction was intermediate in age, and the amino acids and
97 carbohydrates contained a significant contribution of modern carbon. Wang and Druffel (2001) also used this approach and

98 found that the lipids were the oldest compound class from sediments in the Southern Ocean, but the acid insoluble residue was
99 very similar in age to the lipid fraction. These studies suggest that compound classes can have independent cycling rates, but
100 these cycling rates can be influenced by the environment.

101 Here, we apply a ^{14}C compound class approach to soils to more broadly understand SOC turnover mechanisms. We
102 characterize the distribution and ^{14}C age of multiple SOC pools with depth in a well-studied annual grassland in California,
103 using soil physical fractionation (McFarlane et al., 2013; Poeplau et al., 2018) and modified compound class extraction
104 methods previously detailed for marine sediments (Wang et al., 1998). We measured the radiocarbon values of water
105 extractable organic carbon (WEOC), total lipid extracts (TLE), total hydrolysable amino acids (AA), and an acid-insoluble
106 (AI) fraction from bulk and physically separated size fractions (bulk soil, sand, and silt+clay). We expected the TLE to be
107 older than its source fraction (bulk soil, sand, or silt+clay), to be older with depth as the decline in plant inputs necessitates
108 recycling and use of older SOC, and to be older in the silt+clay fraction as its high surface area should result mineral-OC
109 associations that protect SOC from soil microbes. We expected the AA to cycle faster than the TLE fraction and the bulk SOC
110 pool based on the young ^{14}C ages found for AA extracted from in marine sediments (Wang et al., 1998; Wang and Druffel,
111 2001), but hypothesized that recycling of amino acids at depth by soil microbes might result in an increase in the age of AA
112 below 50 cm. Finally, we expected AI to have old C, similar to the TLE, as seen found in marine sediments (Wang et al.,
113 1998). Here, we describe the relative abundance and radiocarbon content of total lipid and amino acid compound class extracts
114 and compare carbon storage and cycling rates within soil size fractions. These data provide a foundation for the continued
115 application of compound class ^{14}C work to the understanding and modelling of soil OC persistence.

116 **2 Materials and Methods**

117 **2.1 Site and Sample Description**

118 Soil samples were collected from the University of California's Hopland Research and Extension Center (HREC) in
119 January 2022. The site is an annual grassland with a Mediterranean-type climate, where the mean annual precipitation (MAP)
120 is 940 mm per year and mean annual temperature is 15°C (Nuccio et al., 2016). The underlying geology consists of mixed
121 sedimentary rock of the Franciscan formation. The soils are designated Typic Haploxeralfs of the Witherall-Squawrock
122 complex (Soil Survey Staff, 2020). The samples were collected from the "Buck" site (39.001° , -123.069°) where the vegetation
123 is dominated by annual wild oat grass, *Avena barbata* (Kotanen, 2004; Bartolome et al., 2007). Soils were collected from a
124 freshly dug soil pit at four depths: 0–10 cm, 10–20 cm, 20–50 cm, and 50–100 cm. The site is dominated by annual grasses,
125 shallow rooted herbs, and forbs, and we did not observe roots below 10 cm. Thus, root derived inputs of OC are important
126 near the soil surface, but do not directly affect deeper soils at this site. Samples were stored in sealed plastic bags at ambient
127 temperature and transported to the laboratory in Livermore, CA. Soil samples were air dried, homogenized, and sieved to 2
128 mm, with the >2 mm fraction retained for further analysis. Samples were subdivided for soil characterization, physical size

129 separations, chemical compound extractions, and density fractionation.

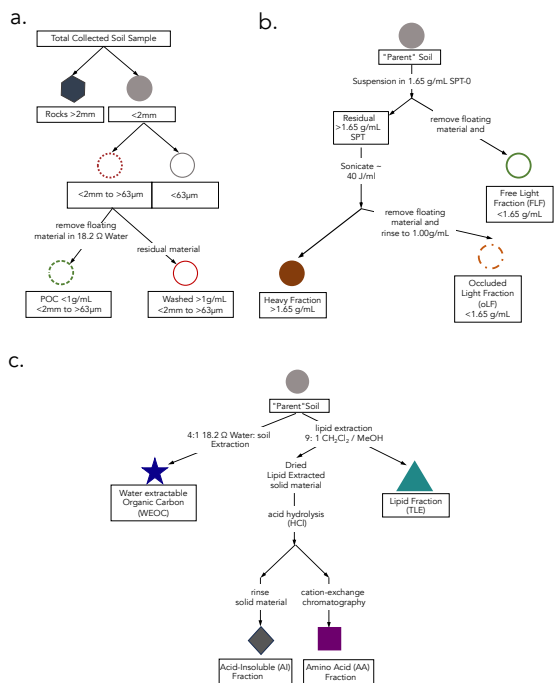
130 **2.2 Physical Fractionation**

131 To compare compound classes between mineral-associated OC and mineral-free OC, we used a salt-free and chemical-
132 free method for isolating the mineral-associated organic matter from the free particulate organic matter (Fig. 1a). Under the
133 assumption that mineral-associated carbon is primarily found in the silt+clay (<63 μm) particle size fraction, we used a size
134 fractionation sieving method where air-dried samples were dry-sieved into three size fractions: bulk soil (<2 mm), sand (2 mm
135 - 63 μm), and silt+clay (<63 μm) (Lavallee et al., 2020; Poeplau et al., 2018). Additionally, because the majority of free
136 particulate organic carbon (POC) is contained in the sand fraction, we used a “water density” separation to remove the low
137 density POC from the mineral matter in this fraction, resulting in a POC (<1g mL⁻¹) fraction and a POC-free (>1g mL⁻¹) sand
138 fraction.

139 To further characterize these soils and aid in interpretation of our data, we compared the size fractionated samples to
140 samples separated by density using sodium polytungstate (SPT-0 adjusted to a density of 1.65 g ml⁻¹) (Poeplau et al., 2018)
141 (see SI Section 1.1 for detailed methods). We chose to focus our compound class extraction efforts on size fractionated samples
142 to avoid chemical alteration of SOC during exposure to SPT.

143 To constrain any contributions of parent materials to SOC, we processed and analyzed the rock fraction (> 2mm) (Agnelli
144 et al., 2002; Trumbore and Zheng, 1996). Rocks were washed with 18.2 M Ω water in an ultrasonic bath to remove surface
145 contamination, rinsed with 1N HCl to remove any additional weathered material loosely adhered to the surface, dried at 60°C,
146 then manually crushed.

147 A large, representative aliquot (~10 g) of the bulk and each physical fraction were ball milled and measured for total
148 organic carbon (TOC, wt %), C/N ratio, $\delta^{13}\text{C}$ and $\Delta^{14}\text{C}$ (Section 2.6). In addition, we analyzed the bulk soils at each depth with
149 nuclear magnetic resonance (¹³C NMR) to assess the broad structural complexity of the OC in the bulk soil (SI Section 2).



151

152

153

154

155

156

157

158

159

160

161

162

163

164

165

166

167

168

Figure 1: Schematics of protocols used in this study for a) fractionation by size, b.) density separation (details in SI methods), and c) extraction of targeted compound classes. The “parent soil” refers to the soil from which the different compound classes are extracted. All compound extractions and physical fractionations were applied to the <2 mm bulk soil; total lipid extract (TLE), amino acid (AA), and acid insoluble (AI) compound classes were also extracted from the silt+clay fraction; and only the TLE was extracted from the dense fraction (DF).

2.3 Water-extractable organic carbon (WEOC)

The water-extractable organic carbon (WEOC) fraction was collected from 80 g of bulk soil with 18.2 MΩ water using a 4:1 water to soil ratio (Van Der Voort et al., 2019; Lechleitner et al., 2016; Hagedorn et al., 2004). Saturated soil samples were shaken for 1 hour and then filtered through a pre-rinsed 0.45 µm polyethersulfone (PES) Supor filter under vacuum. An aliquot was taken for dissolved organic carbon (DOC) measurement on a Shimadzu TOC-L combustion catalytic oxidation instrument. Sample concentrations were determined using a nine-point DOC calibration curve ranging from 0–200 mgC L⁻¹. The WEOC fraction was dried using a Labconco CentriVap centrifugal drying system at 40°C and subsequently transferred with 0.1N HCl into pre-combusted quartz tubes to eliminate any inorganic carbon dissolved in the aqueous fraction. The acidified WEOC fractions were then dried down using the CentriVap. Dried samples were flame sealed under vacuum (Section 2.6) for subsequent carbon isotope analyses.

169 **2.4 Total Lipid Extraction (TLE)**

170 Total lipids (TLE) were extracted from the soil samples using an Accelerated Solvent Extraction (ASE) system (Dionex
171 350, Thermo Scientific) in duplicate. The TLE was extracted from the bulk, sand, silt+clay, and the dense fraction ($> 1.65 \text{ g}$
172 ml^{-1} ; DF). An aliquot of 10–30 g of soil was loaded into a stainless-steel ASE extraction cell depending on TOC content
173 (Rethemeyer et al., 2004). The ASE was set to extract the sample for 5 minutes with a holding temperature of 100°C at 1500
174 PSI. Lipids were extracted using a 9:1 ratio of dichloromethane (DCM or syn: methylene chloride) to methanol (Wang et al.,
175 1998; Van Der Voort et al., 2017; Grant et al., 2022). The TLE was dried under constant ultra-pure N_2 flow at 40°C using a
176 nitrogen dryer (Organomation Multivap Nitrogen Evaporator). The TLE was resuspended in $\sim 5 \text{ ml}$ of 9:1 DCM:Methanol then
177 transferred to pre-combusted quartz tubes, dried again, and analyzed for ^{14}C as described below (Section 2.5). Total CO_2
178 produced by the combustion of the TLE was measured manometrically on the ^{14}C vacuum lines during graphitization. Process
179 blank samples were analyzed with each batch (SI Section 3.1).

181 **2.5 Amino Acid (AA) Extraction**

182 Amino acids (AA) were extracted from the lipid-extracted residual bulk and silt+clay size fraction with an acid hydrolysis
183 procedure, desalted, and isolated with cation exchange chromatography using methods modified from those used in marine
184 systems (Wang et al., 1998; Ishikawa et al., 2018; Blattmann et al., 2020). Briefly, a 500 mg soil aliquot was hydrolyzed with
185 6N HCl (ACS grade) under an N_2 atmosphere for 19-24 hours at 110°C . After hydrolysis, amino acids in solution were
186 separated from the solid acid insoluble (AI) fraction via centrifugation for 5 minutes at 2500 rpm. The AI fraction was
187 subsequently washed at a minimum three additional times with 0.2N HCl to ensure complete AA recovery. The supernatant
188 was collected in a single pre-combusted vial and then filtered through a pre-combusted quartz wool fiber plug to remove
189 extraneous sediment particles. The filtered hydrolysate was dried using a CentriVap at 60°C for 4 hours. The dried supernatant
190 was redissolved in 1 ml 0.1N HCl and loaded onto a preconditioned resin column (BioRad 50WX8 200-400 mesh resin) to
191 isolate the AA from other hydrolyzed organic matter and remove excess chloride. Details of the procedure can be found in
192 Ishikawa et al., 2018. Briefly, once the sample was loaded on the column, it was rinsed with three bed volumes ($\sim 6 \text{ ml}$) of 18.2
193 $\text{M}\Omega \text{ H}_2\text{O}$. The free AA were eluted with 10 ml of 2N ammonium hydroxide (NH_4OH), then transferred into pre-baked quartz
194 tubes, dried at 60°C in the CentriVap, and finally sealed and combusted for isotopic analysis. The remaining rinsed solid
195 residual after hydrolysis is the acid-insoluble (AI) fraction. These are processes as a solid sample for isotopic analysis.

197 **2.6 Isotopic and elemental analysis**

198 All samples were analyzed for radiocarbon (^{14}C) at the Center for Accelerator Mass Spectrometry (CAMS) at Lawrence
199 Livermore National Lab (LLNL) in Livermore, California. Samples were either measured on a 10 MV Van de Graaf FN or
200 1MV NEC Compact accelerator mass spectrometer (AMS) (Broek et al., 2021), with average errors of $F^{14}\text{C} = 0.0035$. For

201 solid soil analysis, 10 to 250 mg of ground material was weighed into a pre-combusted quartz tubes along with 200 mg CuO
202 and Ag, flame sealed under vacuum, then combusted at 900°C for 5 hours. The CO₂ was reduced to graphite on preconditioned
203 iron powder under H₂ at 570°C (Vogel et al., 1984). Measured ¹⁴C values were corrected using δ¹³C values and are reported
204 as age-corrected Δ¹⁴C values using the following the conventions of Stuiver and Polach (1977). Extraneous C was quantified
205 for the TLE and AA extractions (SI Table 4 and SI Section 3). For ease of reference, we included conventional radiocarbon
206 ages in our figures and tables. We quantified turnover times using the single pool turnover model described in Sierra et al.
207 (2014) and Van Der Voort et al. (2019) and explained in detail in Trumbore (2000) and Torn et al. (2009). This approach
208 generates two solutions for pools with Δ¹⁴C > 0 ‰, one corresponding to each side of the atmospheric ¹⁴C-CO₂ curve over the
209 last 70 years (Hua et al., 2022). Unfortunately, we cannot identify the correct solution (McFarlane et al., 2013; Trumbore,
210 2000), especially for TLE and AA fractions from the top 20 cm, as we do not have multiple time points or additional constraints
211 such as pool-specific input or decomposition rates. Therefore, our data analysis and interpretations rely on the reported Δ¹⁴C
212 values. All individual ¹⁴C measurements used in this study are listed in the Supplementary Information (SI Table 1 and 2).
213 For each solid sample, a dried homogenized aliquot was analyzed for TOC concentration and δ¹³C using an elemental analyzer
214 (CHNOS) coupled to an IsoPrime 100 isotope ratio mass spectrometer at the Center for Stable Isotope Biogeochemistry (CSIB)
215 at the University of California, Berkeley. Samples are assumed to have no inorganic carbon based on acid leaching tests and
216 previously published ¹⁴C work at this site (Finstad et al, 2023, Foley et al., 2023). δ¹³C was measured in duplicate for each
217 solid sample and errors represent the standard deviation of the mean. δ¹³C values of WEOC, TLE, and AA extracts were
218 measured on a split of the cryogenically purified CO₂ and were analyzed at the Stable Isotope Geosciences Facility at Texas
219 A&M University on a Thermo Scientific MAT 253 Dual Inlet Stable Isotope Ratio Mass Spectrometer (SI Table 1).

221 **2.7 Data analysis**

222 Data was analyzed using MATLAB version R20223 and R v. 3.614 (R Core Team, 2019). Linear regressions were
223 calculated between the sample depth mid-point and Δ¹⁴C values from both the size fractions as well as the extracted compounds
224 (WEOC, TLE, AA, AI) from the different size fractions. This was done to directly compare the difference in Δ¹⁴C value
225 between the compound classes. Correlation coefficients, p-values and r² are provided in SI Table 3. Analysis of Variance
226 (ANOVA) was used to assess differences in Δ¹⁴C with depth, between TLE and AA, and between soil fractions. ANOVA tests
227 were performed in R v. 3.614 (R Core Team, 2019). In the text, results are reported as means followed by one standard error
228 when n = 2 or 3 or by analytical error when n = 1.

230 **2.8 Interpretation of radiocarbon data**

231 In the interpretation of soil ¹⁴C activity, we must consider how ¹⁴C created during atmospheric nuclear weapons may have
232 affected the isotopic signatures of SOC at our study site. Significantly elevated “bomb” derived ¹⁴C was released into the

233 environment during atmospheric nuclear weapons testing during the mid-20th century. This atmospheric radiocarbon spike has
234 been continuously incorporated into carbon reservoirs including vegetation, soils, and oceans (Levin and Hessshaimer, 2000).
235 Plants assimilate CO₂ with the ¹⁴C signature of the current year's atmosphere during photosynthesis and thus incorporate the
236 current atmospheric ¹⁴C signature into their tissues and root exudates. This signature then cycles into and through soils as this
237 plant-derived organic matter decays, is processed by microbes, and enters stable soil organic matter pools (Torn et al. 2009).
238 Since the termination of atmospheric weapons testing in the 1960s and with continued fossil fuel emissions, the ¹⁴C of
239 atmospheric CO₂ has decreased to approximately pre-1950 values with $0 \pm 1\text{‰}$ reported for the 2019 Northern Hemisphere
240 growing season (Hua et al. 2022). Thus, soil carbon pools with ¹⁴C signatures above 0‰ can be interpreted as decadal-aged or
241 decadal cycling C and pools with ¹⁴C signatures below 0‰ cycle on century to millennial timescales.

242

243 **3 Results**

244 **3.1 Radiocarbon values and characterization of the physical fractions**

245 We used soil size and density fractionation to separate the bulk soil into fractions with different degrees of mineral
246 protection. Radiocarbon content for the bulk soil, sand, and silt+clay (SI Table S3) became more ¹⁴C depleted (older) with
247 increasing depth (Table 1, Fig. 2). SOC in the silt+clay was consistently younger than in the bulk soil, with the average
248 difference in $\Delta^{14}\text{C}$ values increasing from 4‰ at the surface to 87‰ at depth. In the sand fraction, the $\Delta^{14}\text{C}$ values of POC
249 were consistently near current atmospheric values ($2 \pm 3\text{‰}$) and were not significantly correlated with depth. In contrast, the
250 $\Delta^{14}\text{C}$ values of the POC-free sand-sized fraction declined with depth ($25 \pm 3\text{‰}$ to $-510 \pm 2\text{‰}$, $p = 0.006$) and were
251 indistinguishable from the POC-free sand fraction (Fig. 2). Density fractionation of the bulk soil resulted in most of the sample
252 mass (> 98%) and OC (75–83%) recovered in the DF at all depths (SI Fig. S2).

253

254

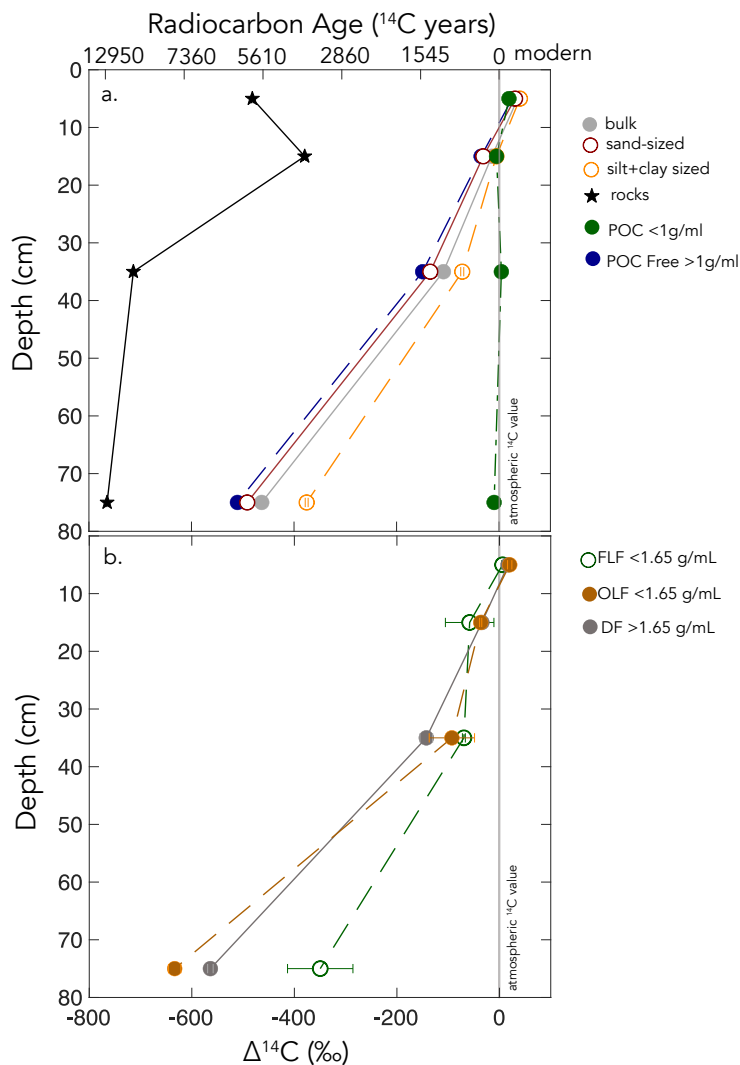
Table 1. Carbon concentrations, mass fractions, and radiocarbon values for the size separations from the Buck Pit

Depth	bulk (<2mm)				sand-sized (2mm to 63 μ m)				silt+clay (<63 μ m)			
	%OC	$\Delta^{14}\text{C} \pm$ errr (‰)	mass <i>f</i>	%OC	$\Delta^{14}\text{C} \pm$ errr (‰)	%OC	$\Delta^{14}\text{C} \pm$ errr (‰)	%OC	$\Delta^{14}\text{C} \pm$ errr (‰)	mass <i>f</i>	%OC	$\Delta^{14}\text{C} \pm$ errr (‰)
0-10 cm	3.14	31 \pm 3	0.71	2.68	25 \pm 3	2.08	25 \pm 3	25.69	19 \pm 3	0.29	4.25	34 \pm 3
10-20 cm	1.22	-22 \pm 3	0.69	0.94	-38 \pm 3	0.77	-35 \pm 3	25.99	-5 \pm 3	0.31	1.84	-13 \pm 3
20-50 cm	0.50	-116 \pm 3	0.75	0.39	-142 \pm 3	0.38	-149 \pm 2	n.m.	4 \pm 3	0.25	0.85	-79 \pm 3
50-100 cm	0.25	-468 \pm 3	0.79	0.23	-496 \pm 3	0.18	-510 \pm 2	n.m.	-10 \pm 3	0.21	0.35	-380 \pm 3

255

256

257



258

259 **Figure 2: $\Delta^{14}\text{C}$ values by depth for a) size-fractions. b) density-fractions from the Buck soil pit. Conventional ^{14}C ages are provided**
260 **for reference.**

261

262

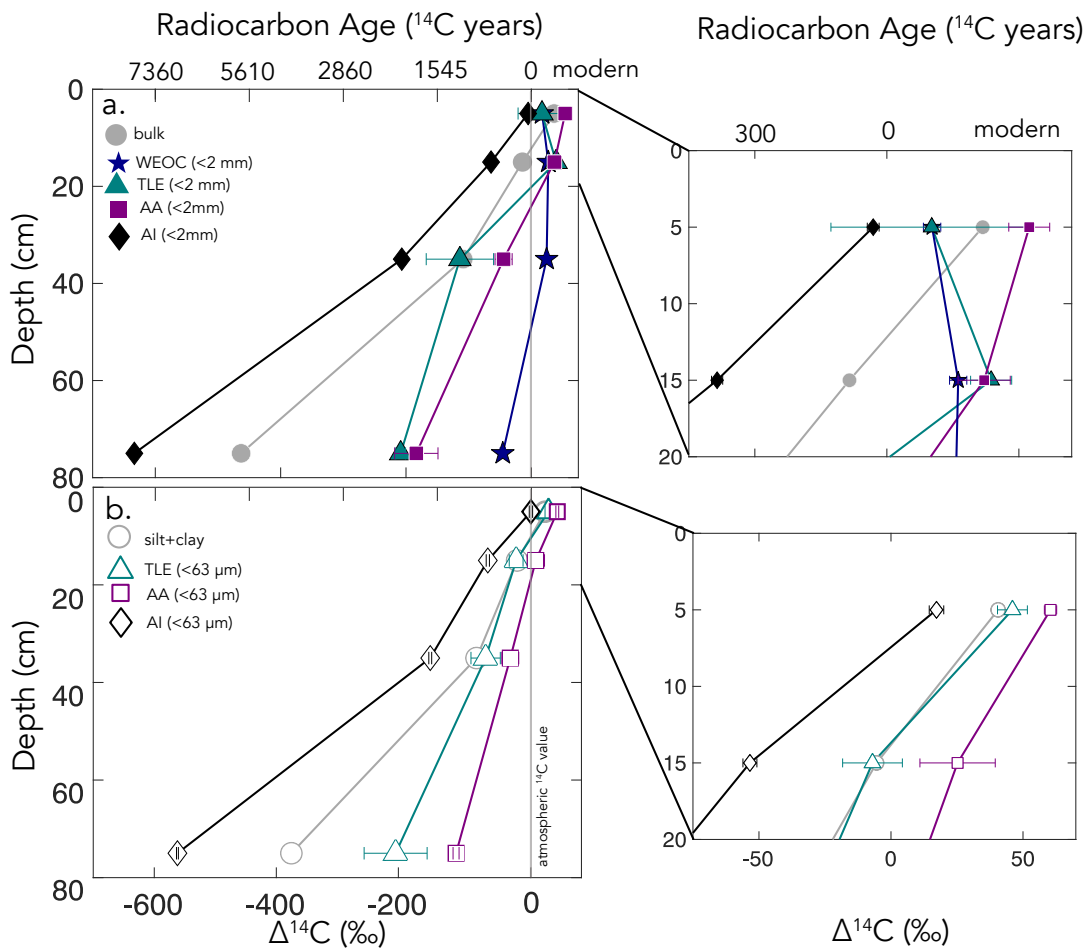
263 3.2 Compound Class results from bulk soil and silt+clay

264 In both the bulk soil and silt+clay fraction, the extracted compound classes became ^{14}C -depleted with depth except for the
265 WEOC, which had ^{14}C values that reflected C inputs recently fixed from the atmosphere throughout the soil profile (Fig. 2; SI

266 tables). The $\Delta^{14}\text{C}$ values of the WEOC ranged from $14 \pm 4\text{‰}$ at the surface to $-46 \pm 4\text{‰}$ at depth, and the DOC concentrations
267 ranged from 43.2 to 6.7 mg C g soil⁻¹ at the surface and at depth, respectively.

268 The TLE from the bulk soil had $\Delta^{14}\text{C}$ values that range from 17 ± 27 to $-208 \pm 6\text{‰}$ ($n = 2$; \pm SE) in the surface and deepest
269 sample, respectively. In comparison, the TLE from the silt+clay fraction was modern at the surface and became more ^{14}C
270 depleted with depth ($p < 0.001$), from 46 ± 4 to $-204 \pm 36 \text{‰}$. The slopes of the linear regressions of $\Delta^{14}\text{C}$ with depth were
271 indistinguishable in TLE from the bulk soil and silt+clay. In addition, the TLE from the bulk TLE and silt+clay fraction TLE
272 (SI Tables) had very similar $\Delta^{14}\text{C}$ values, but the bulk soil had less lipid-C extracted during each experiment ($280 \mu\text{g g C}^{-1}$ in
273 the 0–10 cm vs. $150 \mu\text{g g C}^{-1}$; SI Table 2).

274 The $\Delta^{14}\text{C}$ values of the AA extracted from the bulk soil ranged from 54 ± 5 to -183 ± 24 ($n = 2$, SE) with depth (Fig. 3, SI
275 Table S3). Similarly, the $\Delta^{14}\text{C}$ value of the AA fraction extracted from silt+clay declined with depth from $60 \pm 3\text{‰}$ ($n = 2$, SE)
276 at the surface to $-106 \pm 4 \text{‰}$ ($n = 2$, SE) at 50–100 cm depth. The slopes of the AA extracted from the bulk and silt+clay-size
277 fractions were statistically different, indicating that the AA extracted from the bulk soil became more depleted with depth than
278 that extracted from the silt+clay (SI Table S3). Furthermore, AA fractions were enriched in ^{14}C relative to the TLE or AI
279 fraction ($p < 0.01$ for bulk soil and $p < 0.05$ for silt+clay). The AI fraction was the oldest fraction found in our study at each
280 depth. The $\Delta^{14}\text{C}$ values of the AI fraction ranged from $-5 \pm 2\text{‰}$ to $-633 \pm 2\text{‰}$ (analytical error, $n=1$) and declined with depth
281 ($p < 0.01$) for bulk soil and silt+clay (Fig. 3; SI Table S3).



282
 283 **Figure 3:** a) $\Delta^{14}\text{C}$ by depth for bulk soil and four compound class fractions extracted from bulk soil for the entire depth profile with
 284 the inset of the top 20 cm. b) $\Delta^{14}\text{C}$ by depth for the silt+clay (<63 μm) fraction and three compound classes extracted from the
 285 silt+clay for the entire depth profile with the inset of the top 20 cm. For TLE and AA fractions (n=2) and error bars represent the
 286 standard error from duplicate measurements. For the <2 mm, WEOC, and AI fractions (n=1) and error bars represent analytical
 287 error. Error bars are smaller than the marker width where not shown.
 288

289
 290 **4 Discussion**

291 **4.1 Variability of ^{14}C in compound classes in soils**

292 We measured radiocarbon content of four distinct soil chemical extracts: water extractable organic carbon (WEOC), total
 293 lipid extract (TLE), free amino acids (AA), and the acid insoluble fraction (AI), each of which had distinct $\Delta^{14}\text{C}$ values
 294 compared to the parent soil it was extracted from (bulk or silt+clay; Fig. 4a and 4b). The central questions of this study are:

295 What are the differences in cycling time/age between various organic compounds in the soil? Do these differences in cycling
296 time change with depth? As expected, $\Delta^{14}\text{C}$ values of TLE, AA, and AI became more depleted with depth (Fig. 2). More
297 interestingly, the differences between the ^{14}C content of parent soil and the extracted compounds were not consistent with
298 depth (Fig. 3a and 3b). This divergence in $\Delta^{14}\text{C}$ values reflects differences in turnover times among compound classes, which
299 can be influenced by the sources of OC to each of these pools and by differences in the stabilization mechanisms protecting
300 those compounds from decay. In this annual grassland, plant inputs should have a greater influence on SOC pools near the
301 surface, which we confirmed with near modern $\Delta^{14}\text{C}$ signatures in the 0–10 cm depth for all compound classes and size
302 fractions (Fig. 3b and 3c). Furthermore, at deeper depths, new vegetation inputs should be less readily available, which results
303 in more depleted $\Delta^{14}\text{C}$ signatures at depth and could necessitate microbial use and recycling of older SOC.

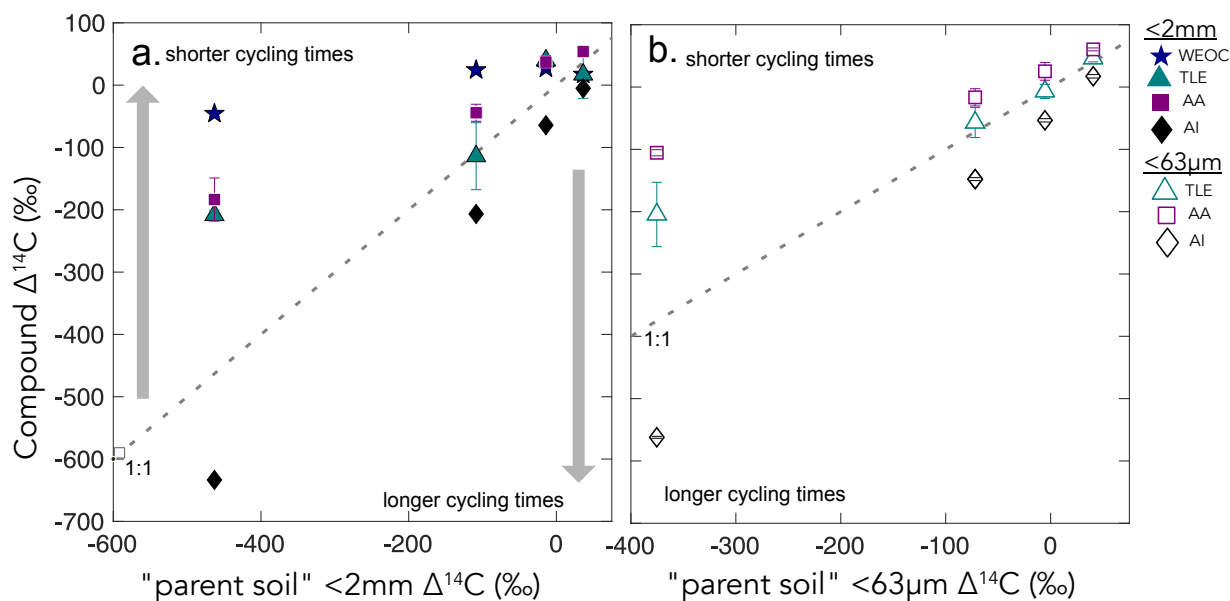
304 We found that, averaged across depths, the $\Delta^{14}\text{C}$ values of the TLE were more depleted than those of the AA, though both
305 compound classes were more enriched in $\Delta^{14}\text{C}$ than the bulk soil or silt+clay from which they were extracted. The extracted
306 AAs are the foundational units of hydrolysed proteins and found in both plant and microbial biomass (Blattmann et al., 2020).
307 As in marine studies, we found the AAs to be the youngest compound class fraction (of the TLE and AI) in these soils. The
308 AA pool likely reflects a more actively cycling microbial pool especially at depth, as AA are enriched in nitrogen compounds
309 and likely microbes are both preferentially mining and recycling these compounds (Moe, 2013). The divergence from bulk ^{14}C
310 values indicate that even at depth in the soil, the AAs are either continuously replenished from transport of AAs from surface
311 horizons or re-synthesized with relatively ^{14}C enriched sources such as the WEOC.

312 Based on published data for both soils and marine sediments, we expected the TLE to be older than both the AAs and the
313 bulk soil, however we found that all TLE samples, no matter what fraction we measured, were more ^{14}C enriched than the bulk
314 soil. TLE is composed of a continuum of lipids from plant and microbial materials, ranging from leaf waxes to microbial cell
315 structural components (Angst et al., 2021; Angst et al., 2016), that cycle at different rates and likely interact with mineral
316 surfaces. Previous studies where individual lipid biomarker $\Delta^{14}\text{C}$ values were measured in soils on either short chain or long
317 chain fatty acids found a divergence in $\Delta^{14}\text{C}$ values between these two pools, with short chain lipids generally having enriched
318 ^{14}C values and long chain lipids having more depleted ^{14}C values (Grant et al., 2022; Van Der Voort et al., 2017). For example,
319 long-chain lipid biomarkers, primarily thought to be plant derived, had consistently older ^{14}C ages than bulk soil (Van Der
320 Voort et al., 2017). Short-chain lipids, which can be microbial or root derived (Rethemeyer et al., 2004), were found to be
321 younger than long-chain lipids throughout the soil profiles and younger than bulk soil at depth (Van Der Voort et al., 2017).
322 However, microbial cell wall lipid biomarkers (glycerol dialkyl glycerol tetraethers, GDGTs) had older ^{14}C ages than bulk
323 soils (Gies et al., 2021). With this consideration, our result of more enriched ^{14}C of the TLE could be an indication of a
324 predominance of short chain lipids and suggested higher abundance of microbially-derived lipids than plant-derived lipids.
325 However further study of specific lipid abundance (e.g., *n*-alkanes, fatty acids) in these soils are necessary, as it is unclear to
326 what degree lipids are older than bulk soils with depth because of preservation of these compounds through mineral association

327 or because of microbial use of aged OC sources for growth.

328 We found that AI, the residual sample after both the TLE and AA have been extracted (Wang et al., 1998; Wang et al.,
329 2006). was the most ^{14}C depleted OC fraction measured at each soil depth (Fig. 3, 4) The AI fraction was far more depleted
330 relative to the bulk soil (Fig. 3a and 4a) than observed in marine studies with acid-insoluble OC (Wang et al., 2006; Wang and
331 Druffel, 2001). In these marine studies, the ^{14}C of the AI varied in age depending on sampling depth and location. The
332 significant depletion of the AI in our soils suggests that these chemically stable compounds are not oxidized in soil.
333 Importantly, our AI samples are older than the other chemical and physical soil fractions that we measured in the soil,
334 consistent with the general expectation that aromatic compounds can be difficult to degrade in in soils (Ukalska-Jaruga et al.,
335 2019).

336



337

338 **Figure 4.** $\Delta^{14}\text{C}$ values of the three extracted compound classes (y-axis) compared to the $\Delta^{14}\text{C}$ values of the parent or source fraction
339 (x-axis) for a) bulk soil and b) silt+clay. The grey dashed lines show the 1:1 line where bulk sample $\Delta^{14}\text{C}$ equals compound class
340 $\Delta^{14}\text{C}$. Gray arrows point to regions where data plot above or below the 1:1 line, suggesting that a given compound class has shorter
341 and longer carbon turnover times than bulk soil, respectively.

342

343 4.2 Differential OC cycling between the different “parent” fractions

344 Our results suggest different OC cycling timescales for the different physical fractions representing the “parent” fractions.
345 Here, we focus on the silt+clay fraction as an operationally defined mineral-associated OC pool. Numerous soil physical

346 fractionation schemes have been applied to soils and disparities in methods challenge interpretation and intercomparison of
347 results from different studies using different approaches. We compared the size-based soil fractionation to the density
348 fractionation to aid in interpretation and comparability of our findings to other studies. Our silt+clay fraction had higher $\Delta^{14}\text{C}$
349 values than the sand, POC-free sand, and the DF. Our silt+clay fraction could include free organic matter that passed through
350 the 63 μm sieve but that would have floated off the DF during density fractionation. For reference, the FLF has higher $\Delta^{14}\text{C}$
351 values than the mineral-associated pools and bulk soils (Fig. 5), but also has high C:N reflecting the high OC content and
352 dominantly plant origin of this fraction (SI Table S1). We assume that this small-size free OC is a small fraction of the total
353 silt+clay OC as no small fragments of organic matter were visible and because the C:N ratios of the silt+clay fractions are only
354 slightly elevated compared to the bulk soil and sand fractions (SI Table S1). Rather, the silt+clay fractions may have higher
355 $\Delta^{14}\text{C}$ values relative to the POC-free sand and bulk soil because higher surface area in the silt+clay may facilitate mineral
356 association with surface derived OC with minerals (e.g., from the WEOC fraction).

357 Additionally, our TLE comparison between different size and density fractions highlights the important influence that
358 method selection has over experimental results. The mineral-associated TLE cycled more rapidly than the bulk soil no matter
359 which “mineral-associated” fraction (the silt+clay or the DF) was chosen (Fig. 6). The $\Delta^{14}\text{C}$ values of TLE from the bulk,
360 sand, and silt+clay fractions were indistinguishable from one another, possibly because the size fractionation scheme did not
361 effectively separate distinct lipid pools. However, the $\Delta^{14}\text{C}$ values of TLE from the DF were significantly more ^{14}C depleted
362 than TLE from the silt+clay size fraction (Fig. 6), suggesting there were older lipids in the DF relative to the silt+clay.
363 However, more depleted ^{14}C values found in the TLE from the DF compared to the silt+clay could have resulted from the DF
364 being exposed to SPT and/or ground after drying and before lipid extraction. It is possible that grinding the DF prior to lipid
365 extraction increased the exposed surface area and resulted in a larger fraction of old SOC or rock-derived OC being
366 incorporated into the TLE than if the DF had not been ground. Clearly, the approach used to fractionate soils influences
367 experimental results and must be considered when interpreting differences in persistence across operationally defined OC
368 pools.

369

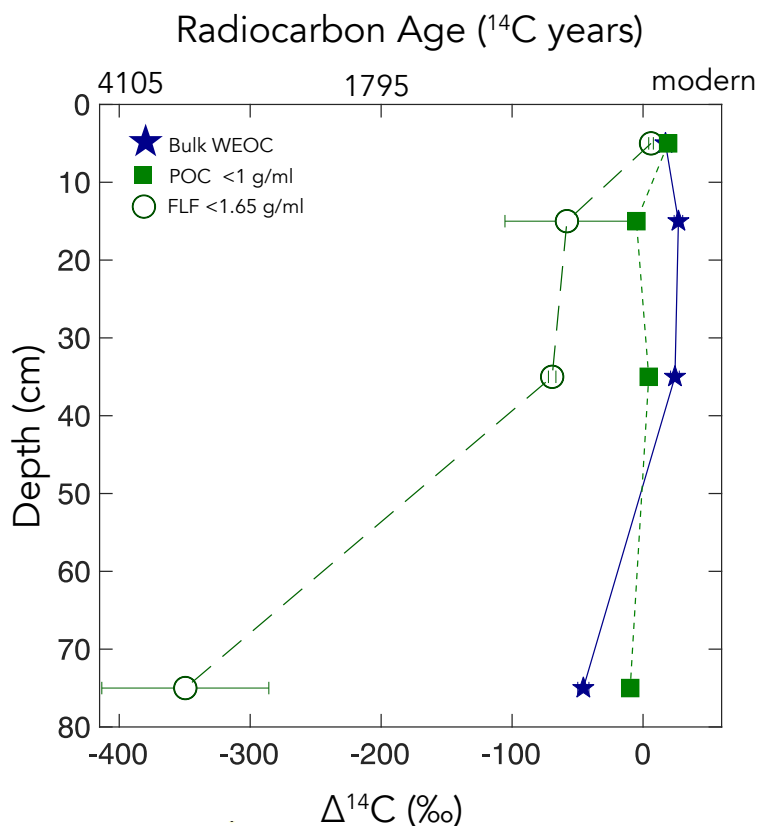
370 4.3 Variation in OC cycling throughout the depth profile

371 The WEOC (extracted from bulk soils) and POC ($<1\text{g mL}^{-1}$ floated off the sand-size fraction) had the highest $\Delta^{14}\text{C}$ values
372 throughout the soil profile, reflecting a predominance of modern carbon from plant detritus and root exudates to these pools.
373 WEOC fractions can comprise a complex mixture of molecules with different structures (Hagedorn et al., 2004; Bahureksa et
374 al., 2021), which are common only in their ability to be mobilized and dissolved in water. WEOC can mobilize and percolate
375 down the soil profile with sufficient precipitation to allow vertical transport. Both the POC and WEOC fractions supply OC
376 that is readily accessible for microbial degradation and microbial utilization – resulting in the rapid turnover and relatively
377 high $\Delta^{14}\text{C}$ values of these two pools (Marin-Spiotta et al., 2011). Occurrence of young OC in deep soils may be driven by

378 microbial uptake of this young and bioavailable DOC or POC. Additionally, we found that the free light-density fractions were
379 depleted in ^{14}C relative to the WEOC and POC (Fig. 5). We suspect this is due to colloidal particles in the FLF, which are not
380 dispersed or dense enough to settle in the SPT.

381 The study site has a Mediterranean climate, and these soils undergo seasonal wetting and drying cycles that may intensify
382 in the future (Swain et al., 2018), potentially shifting the composition or amount of OC that percolates down the soil column.
383 When soil is already moist, subsequent rainfall may mobilize both OC and colloidal sized mineral material under reducing
384 conditions, which may interact to form stable mineral-OC colloids that can enhance the transport of OC down the soil profile
385 and out of the system (Buettner et al., 2014). With prolonged dry periods, water soluble OC may be more susceptible to
386 microbial decomposition or oxidation because anaerobic preservation is removed (Heckman et al. 2022) This seasonal wetting
387 and drying mechanism likely controls what types of organic matter are transported down the soil profile. Deeper in the soil
388 profile, greater reactive mineral surface area and lower microbial activity can enhance carbon stabilization in subsoils (Homyak
389 et al., 2018; Dwivedi et al., 2017; Pries et al., 2023). Further research is needed to understand the effects of seasonal wetting
390 and drying on the behaviour of water-soluble OC in the soil profile.

391 In general, the $\Delta^{14}\text{C}$ values of the TLE, AA, and AI decreased with increasing depth in the profile. While all extracted
392 compounds followed this trend, the degree of ^{14}C depletion with depth varied somewhat between the different compound
393 classes and between the bulk and silt+clay parent fractions. The TLE extracted from the bulk and from the silt+clay fraction
394 had similar slopes with depth. This suggests that depth has more influence than fraction size on resulting lipid ^{14}C content,
395 possibly because of limited transport of lipids down the soil profile. The AAs extracted from the bulk and the silt+clay fraction
396 differed from one another in that the AA extracted from the bulk soil became more depleted with depth than the AA extracted
397 from the silt+clay. This suggests that at depth, AAs from the silt+clay fraction cycle more quickly than AA's extracted from
398 the bulk soil, possibly indicating that the silt+clay fraction is more directly influenced by microbial activity than the sand
399 fraction. At depths greater than 30 cm, the TLE and AA fraction were markedly younger than the bulk soil, possibly resulting
400 from transport of lipids and amino acids from surface horizons down profile, rapid recycling of these compounds at depth, the
401 use of a relatively modern C source for lipid and amino acid synthesis at depth, or most likely, a combination of these. At all
402 depths the AI was significantly older than the parent fraction, indicating that throughout the soil profile the AI contains an old
403 and stable pool of OC.



404
 405 **Figure 5: POC (floated from the sand, n = 1), FLF (from bulk soil, n = 3, and error bars indicate standard error on the mean), and**
 406 **WEOC (from bulk soil, n=1). $\Delta^{14}\text{C}$ values by depth. For POC and WEOC, error bars indicate analytical error are generally smaller**
 407 **than the symbols.**
 408

409 4.4 Compound class $\Delta^{14}\text{C}$ values in mineral-associated SOC

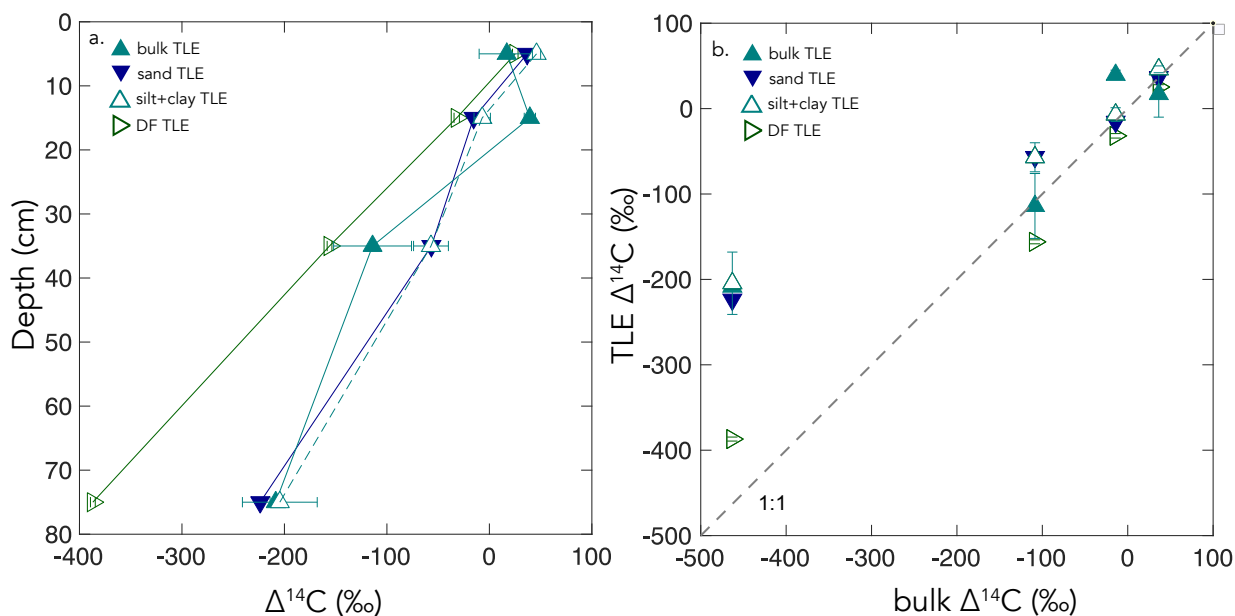
410 To investigate the effect of mineral interaction on the $\Delta^{14}\text{C}$ values or persistence of the TLE, AA, and AI, we measured
 411 these extracted compound classes from physical fractions intended to yield approximate mineral-associated carbon pools. We
 412 focused primarily on the silt+clay size fraction as the physical fraction that best approximates a mineral-associated OC pool
 413 derived from microbially processed plant inputs (Poeplau et al., 2018; Lavallee et al., 2020) and assume that after size
 414 fractionation most of the free organic matter in the bulk soil was in the sand size fraction. We compared the silt+clay size
 415 fraction $\Delta^{14}\text{C}$ values to the bulk $\Delta^{14}\text{C}$ values to determine if the material extracted from the isolated mineral-associated fractions
 416 of the soil had greater OC persistence or if these compounds cycled indiscriminate of mineral association (Fig. 2).

417 While the TLE from the silt+clay and bulk soil had similar $\Delta^{14}\text{C}$ values, the AA from the silt+clay size fraction was
 418 enriched in ^{14}C compared to the AA from bulk soil ($r^2 = 0.98$, $p < 0.05$). This suggests that AAs cycle faster in the silt+clay

419 mineral pool than in the bulk soils. While mineral surfaces usually are thought to promote stability and persistence of OC, in
420 some soil systems, mineral associations may not be the single defining factor of OC persistence (Rocci et al., 2021) and could
421 have a more nuanced role influencing OC cycling in soils.

422 Our data suggests there is a continuum of compounds that exist with different ^{14}C values in the mineral-associated pool,
423 because in the silt+clay fraction, the TLE, AA, and AI have significantly different ^{14}C values (Fig. 4b). For instance, the
424 mineral-associated TLE and AA fractions are enriched in ^{14}C relative to the silt+clay fraction, suggesting both are cycling
425 faster than the average mineral associated pool. However, the AI from the silt+clay fraction is cycling slower than solid sample
426 it was extracted from, and when we compare the AI from the bulk soil to the AI from the silt+clay, the AI from the silt+clay
427 is slightly more ^{14}C enriched. This suggests that there is slight ^{14}C enrichment across compounds in the silt+clay fraction
428 relative to sand and bulk soil.

429 We also compared the TLE extracted from the silt+clay to that extracted from the DF because both fractions are often
430 considered mineral associated. Across studies, the mineral-associated OC is not a uniformly defined pool, and the observed
431 results are a consequence of the methodology used to separate the samples (Fig. 6). The DF TLE $\Delta^{14}\text{C}$ is significantly older
432 than the silt+clay TLE (Fig. 6b) and the TLE of the bulk soil at depth (Fig. 6). This suggests that lipids in mineral-associated
433 OC pools vary in cycling rates. This is complementary to findings from other studies where ^{14}C values from different lipid
434 biomarkers are divergent from the bulk soils (Gies et al., 2021) and indicates the necessity of looking at entire compound class
435 pools for understanding soil carbon persistence. Further investigation into the composition and age-distribution of compounds
436 within mineral associated-OC is needed to better quantify the distribution of cycling rates within mineral associated OC pools.



437

438 **Figure 6: a) $\Delta^{14}\text{C}$ versus soil depth measured for TLE extractions from four soil size/density fractions. b) A comparison of the bulk**
 439 **soil $\Delta^{14}\text{C}$ values to the TLE from the four size/density fractions.**

440

441 4.5 Persistent and Petrogenic OC

442 The most persistent, oldest OC was found in the AI fraction. Because carbon in the AI cycles more slowly than other
 443 components of this grassland soil, it is important to understand what structural components make up the AI and where these
 444 compounds are sourced from. The chemical structure of the AI fraction has been difficult to characterize. Hwang and Druffel
 445 (2003) argued that the AI is a lipid-like portion of the ocean OC. However, in soils, the AI can be composed of a mixture of
 446 lipid-like compounds and aromatic compounds (Silveira et al., 2008). In our soil, the ^{13}C -NMR spectra of the AI from 0–10
 447 cm depth show a significant, broad peak in the 100–165 ppm range, indicative of aromatics (SI Fig. 3) (Baldock and Preston,
 448 1995; Baldock et al., 1997). While it is possible that some condensed aromatic compounds form during the hydrolysis
 449 procedure used to remove AAs, the AI may also contain naturally occurring aromatic compounds that could include pyrogenic
 450 or petrogenic OC.

451 The parent material of our site is a mixture of sandstone, shale, greywacke, and schist (Foley et al., 2022), so it is possible
 452 that some of the OC in our soils is ancient, rock-derived, petrogenic carbon that has been incorporated into the soil profile
 453 through pedogenesis progresses (Grant et al., 2023). Comparison of the AI to the rock (>2 mm) fraction shows that the AI is
 454 younger than the OC contained in the rock fraction (SI Table 1), with the rock fraction $\Delta^{14}\text{C}$ values ranging from -481 to -
 455 765‰. To calculate the contribution of OC_{petro} into the AI fraction, we used a binary mixing model with endmembers of

456 OC_{petro} and aged SOC based on the method in Grant et al. (2023). The $\Delta^{14}\text{C}$ value of the OC_{petro} ^{14}C endmember is -1000 ‰
457 and the $\Delta^{14}\text{C}$ value of the biospheric endmember was set as either the measured TLE $\Delta^{14}\text{C}$ value or the bulk $\Delta^{14}\text{C}$ value from
458 each depth. This comparison of these two different biospheric endmembers allowed us to calculate a possible range of values
459 for the OC_{petro} contribution (Table 1). In the AI extracted from the silt+clay fraction, the OC_{petro} contribution was 4–5% from
460 0–10 cm depth and 40–53 % in the 50–100cm depth. In AI extracted from the bulk soil, the OC_{petro} contribution was 0–1 % in
461 the 0–10 cm depth, and 17–44 % in the 50–100 cm depth. Therefore, while the AI fraction likely contains OC_{petro}, it is primarily
462 composed of OC compounds derived from more recent plant and microbial inputs that are highly resistant to acid hydrolysis
463 either because of their chemical structure or their strong associations with minerals.

465 **5 Conclusions and Continued soil radiocarbon compound class characterization**

466 In this study, we characterized a soil carbon profile using compound-class ^{14}C analyses. We found that our extraction
467 methods yielded fractions with ^{14}C signatures distinctly different from the parent soil from which they were extracted. We
468 found that in this annual grassland soil, the AA and the TLE fractions cycle more rapidly than the bulk soil throughout the soil
469 profile. At each depth, the AI fraction is the oldest fraction and contains a combination of slowly cycling SOC and ancient
470 petrogenic C. These results show that soil compound classes cycle differently than similar components in marine systems. Our
471 results also show that mineral-associated SOC contains a mixture of carbon compounds with distinctly different ages and
472 sources that drive turnover and persistence. Compound-specific ^{14}C approaches hold promise for improving our understanding
473 of the chemical structure of SOC, as well as the connection between carbon degradation and preservation in soils. A molecule-
474 resolved understanding of the relationship between compound classes and carbon persistence will also give insight into the
475 fate and turnover time of specific organic biomarkers found in plant residues or the biomass of bacteria, fungi and microfauna.
476 These techniques can also help to determine mechanisms promoting mineral stabilization of soil carbon, especially when
477 combined with soil physical fractionation.

478 Results from this study highlight that radiocarbon measurements of specific organic compounds and compound classes in
479 soil provide valuable insights into the persistence and decomposition rates of soil organic carbon. To improve our ability to
480 model the future of soil carbon stocks and soil quality in the face of a changing global climate, we need further research that
481 interrogates the composition, radiocarbon content, and cycling rates of soil organic carbon and mechanistically links these
482 rates to physical and chemical drivers.

484 **6 Acknowledgements**

485 This work was performed under the auspices of the U.S. Department of Energy by Lawrence Livermore National Laboratory
486 under Contract DE-AC52-07NA27344 and was supported by the LLNL LDRD Program under Project No. 21-ERD-021 and
487 Project No. 24SI002. LLNL-JRNL-843138. Additional support for site access, sample collection, and site characterization

488 data was provided by the U.S. Department of Energy, Office of Biological and Environmental Research, Genomic Sciences
489 Program LLNL ‘Microbes Persist’ Scientific Focus Area (award #SCW1632). We acknowledge the traditional, ancestral,
490 unceded territory of the Shóqowa and Hopland People, on which this research was conducted. We thank the staff at the Hopland
491 Research and Extension Center who manage the experiment site and Z Kagely for his assistance in digging the soil pit.

492

493 **7 Supplemental Tables/Data Availability**

494 A list of all radiocarbon data, stable carbon, and total OC values with a CAMS tracking number for each of the analyses
495 used in this publication.

496 **8 Author Contributions:** KJM, KMF, TABB, JP, and KEG conceptualized the study. KJM, KMF, TABB, JP secured funding
497 for the project. KEG designed the method and carried out the extractions with input from KJM, KMF, and TABB. CJL carried
498 out the density separations. MNR carried out the water extractions. JDK and MM ran the NMR experiments. KEG, KJM,
499 KMF interpreted the data. KEG prepared the paper with contributions of all co-authors.

500

501 **9 Competing interests.** The authors declare that they have no conflict of interest.

502

503

504 **References**

505

506 Agnelli, A., Trumbore, S. E., Corti, G., and Ugolini, F. C.: The dynamics of organic matter in rock fragments in soil
507 investigated by ¹⁴C dating and measurements of ¹³C, *European Journal of Soil Science*, 53, 147-159,
508 <https://doi.org/10.1046/j.1365-2389.2002.00432.x>, 2002.

509 Angst, G., Mueller, K. E., Nierop, K. G. J., and Simpson, M. J.: Plant- or microbial-derived? A review on the molecular
510 composition of stabilized soil organic matter, *Soil Biology and Biochemistry*, 156, 10.1016/j.soilbio.2021.108189, 2021.

511 Angst, G., John, S., Mueller, C. W., Kögel-Knabner, I., and Rethemeyer, J.: Tracing the sources and spatial distribution of
512 organic carbon in subsoils using a multi-biomarker approach, *Scientific Reports*, 6, 1-12, 2016.

513 Bahureksa, W., Tfaily, M. M., Boiteau, R. M., Young, R. B., Logan, M. N., McKenna, A. M., and Borch, T.: Soil Organic
514 Matter Characterization by Fourier Transform Ion Cyclotron Resonance Mass Spectrometry (FTICR MS): A Critical Review
515 of Sample Preparation, Analysis, and Data Interpretation, *Environmental Science & Technology*, 55, 9637-9656,
516 [10.1021/acs.est.1c01135](https://doi.org/10.1021/acs.est.1c01135), 2021.

517 Baldock, J. A. and Preston, C. M.: Chemistry of Carbon Decomposition Processes in Forests as Revealed by Solid-State
518 Carbon-13 Nuclear Magnetic Resonance, in: *Carbon Forms and Functions in Forest Soils*, 89-117,
519 <https://doi.org/10.2136/1995.carbonforms.c6>, 1995.

- 520 Baldock, J. A., Oades, J. M., Nelson, P. N., Skene, T. M., Golchin, A., and Clarke, P.: Assessing the extent of decomposition
521 of natural organic materials using solid-state ^{13}C NMR spectroscopy, *Soil Research*, 35, 1061-
522 1084, <https://doi.org/10.1071/S97004>, 1997.
- 523 Bartolome, J. W., James Barry, W., Griggs, T., and Hopkinson, P.: 367Valley Grassland, in: *Terrestrial Vegetation of*
524 *California*, edited by: Barbour, M., University of California Press, 0, 10.1525/california/9780520249554.003.0014, 2007.
- 525 Blattmann, T. M., Montluçon, D. B., Haghypour, N., Ishikawa, N. F., and Eglinton, T. I.: Liquid Chromatographic Isolation
526 of Individual Amino Acids Extracted From Sediments for Radiocarbon Analysis, *Frontiers in Marine Science*, 7,
527 10.3389/fmars.2020.00174, 2020.
- 528 Bour, A. L., Walker, B. D., Broek, T. A. B., and McCarthy, M. D.: Radiocarbon Analysis of Individual Amino Acids:
529 Carbon Blank Quantification for a Small-Sample High-Pressure Liquid Chromatography Purification Method, *Analytical*
530 *Chemistry*, 88, 3521-3528, 10.1021/acs.analchem.5b03619, 2016.
- 531 Broek, T. A. B., Ognibene, T. J., McFarlane, K. J., Moreland, K. C., Brown, T. A., and Bench, G.: Conversion of the
532 LLNL/CAMS 1 MV biomedical AMS system to a semi-automated natural abundance ^{14}C spectrometer: system
533 optimization and performance evaluation, *Nuclear Instruments and Methods in Physics Research Section B: Beam*
534 *Interactions with Materials and Atoms*, 499, 124-132, 10.1016/j.nimb.2021.01.022, 2021.
- 535 Buettner, S. W., Kramer, M. G., Chadwick, O. A., and Thompson, A.: Mobilization of colloidal carbon during iron reduction
536 in basaltic soils, *Geoderma*, 221-222, 139-145, <https://doi.org/10.1016/j.geoderma.2014.01.012>, 2014.
- 537 Coppola, A. I., Wiedemeier, D. B., Galy, V., Haghypour, N., Hanke, U. M., Nascimento, G. S., Usman, M., Blattmann, T.
538 M., Reisser, M., Freymond, C. V., Zhao, M., Voss, B., Wacker, L., Schefuß, E., Peucker-Ehrenbrink, B., Abiven, S.,
539 Schmidt, M. W. I., and Eglinton, T. I.: Global-scale evidence for the refractory nature of riverine black carbon, *Nature*
540 *Geoscience*, 11, 584-588, 10.1038/s41561-018-0159-8, 2018.
- 541 De Troyer, I., Amery, F., Van Moorleghe, C., Smolders, E., and Merckx, R.: Tracing the source and fate of dissolved
542 organic matter in soil after incorporation of a ^{13}C labelled residue: A batch incubation study, *Soil Biology and*
543 *Biochemistry*, 43, 513-519, <https://doi.org/10.1016/j.soilbio.2010.11.016>, 2011.
- 544 Douglas, P. M. J., Pagani, M., Eglinton, T. I., Brenner, M., Curtis, J. H., Breckenridge, A., and Johnston, K.: A long-term
545 decrease in the persistence of soil carbon caused by ancient Maya land use, *Nature Geoscience*, 11, 645-649,
546 10.1038/s41561-018-0192-7, 2018.
- 547 Dwivedi, D., Riley, W., Torn, M., Spycher, N., Maggi, F., and Tang, J.: Mineral properties, microbes, transport, and plant-
548 input profiles control vertical distribution and age of soil carbon stocks, *Soil Biology and Biochemistry*, 107, 244-259, 2017.
- 549 Eglinton, T. I., Galy, V. V., Hemingway, J. D., Feng, X., Bao, H., Blattmann, T. M., Dickens, A. F., Gies, H., Giosan, L.,
550 Haghypour, N., Hou, P., Lupker, M., McIntyre, C. P., Montluçon, D. B., Peucker-Ehrenbrink, B., Ponton, C., Schefuß, E.,
551 Schwab, M. S., Voss, B. M., Wacker, L., Wu, Y., and Zhao, M.: Climate control on terrestrial biospheric carbon turnover,
552 *Proc Natl Acad Sci U S A*, 118, 10.1073/pnas.2011585118, 2021.
- 553 Feng, X., Vonk, J. E., Griffin, C., Zimov, N., Montluçon, D. B., Wacker, L., and Eglinton, T. I.: ^{14}C Variation of Dissolved
554 Lignin in Arctic River Systems, *ACS Earth and Space Chemistry*, 1, 334-344, 10.1021/acsearthspacechem.7b00055, 2017.

555 Feng, X., Benitez-Nelson, B. C., Montluçon, D. B., Prah, F. G., McNichol, A. P., Xu, L., Repeta, D. J., and Eglinton, T. I.:
556 ¹⁴C and ¹³C characteristics of higher plant biomarkers in Washington margin surface sediments, *Geochimica et*
557 *Cosmochimica Acta*, 105, 14-30, <https://doi.org/10.1016/j.gca.2012.11.034>, 2013.

558 Foley, M. M., Blazewicz, S. J., McFarlane, K. J., Greenlon, A., Hayer, M., Kimbrel, J. A., Koch, B. J., Monsaint-Queeney,
559 V., Morrison, K., Morrissey, E., Hungate, B. A., and Pett-Ridge, J.: Active populations and growth of soil microorganisms
560 are framed by mean annual precipitation in three California annual grasslands, *Soil Biology and Biochemistry*, 108886,
561 <https://doi.org/10.1016/j.soilbio.2022.108886>, 2022.

562 Galy, V., Peucker-Ehrenbrink, B., and Eglinton, T.: Global carbon export from the terrestrial biosphere controlled by
563 erosion, *Nature*, 521, 204-207, [10.1038/nature14400](https://doi.org/10.1038/nature14400), 2015.

564 Galy, V., Beyssac, O., France-Lanord, C., and Eglinton, T.: Recycling of Graphite During Himalayan Erosion: A Geological
565 Stabilization of Carbon in the Crust, *Science*, 322, 943-945, [doi:10.1126/science.1161408](https://doi.org/10.1126/science.1161408), 2008.

566 Gaudinski, J. B., Trumbore, S. E., Davidson, E. A., and Zheng, S.: Soil carbon cycling in a temperate forest: radiocarbon-
567 based estimates of residence times, sequestration rates and partitioning of fluxes, *Biogeochemistry*, 51, 33-69,
568 [10.1023/A:1006301010014](https://doi.org/10.1023/A:1006301010014), 2000.

569 Gies, H., Hagedorn, F., Lupker, M., Montluçon, D., Haghypour, N., van der Voort, T. S., and Eglinton, T. I.: Millennial-age
570 glycerol dialkyl glycerol tetraethers (GDGTs) in forested mineral soils: ¹⁴C-based evidence for stabilization of microbial
571 necromass, *Biogeosciences*, 18, 189-205, [10.5194/bg-18-189-2021](https://doi.org/10.5194/bg-18-189-2021), 2021.

572 Gleixner, G.: Soil organic matter dynamics: a biological perspective derived from the use of compound-specific isotopes
573 studies, *Ecological Research*, 28, 683-695, 2013.

574 Grant, K. E., Hilton, R. G., and Galy, V. V.: Global patterns of radiocarbon depletion in subsoil linked to rock-derived
575 organic carbon, *Geochemical Perspectives Letters*, 25, 36-40, <https://doi.org/10.7185/geochemlet.2312>, 2023.

576 Grant, K. E., Galy, V. V., Haghypour, N., Eglinton, T. I., and Derry, L. A.: Persistence of old soil carbon under changing
577 climate: The role of mineral-organic matter interactions, *Chemical Geology*, 587, [10.1016/j.chemgeo.2021.120629](https://doi.org/10.1016/j.chemgeo.2021.120629), 2022.

578 Hagedorn, F., Saurer, M., and Blaser, P.: A ¹³C tracer study to identify the origin of dissolved organic carbon in forested
579 mineral soils, *European Journal of Soil Science*, 55, 91-100, <https://doi.org/10.1046/j.1365-2389.2003.00578.x>, 2004.

580 Hein, C. J., Usman, M., Eglinton, T. I., Haghypour, N., and Galy, V. V.: Millennial-scale hydroclimate control of tropical
581 soil carbon storage, *Nature*, 581, 63-66, [10.1038/s41586-020-2233-9](https://doi.org/10.1038/s41586-020-2233-9), 2020.

582 Homyak, P. M., Blankinship, J. C., Slessarev, E. W., Schaeffer, S. M., Manzoni, S., and Schimel, J. P.: Effects of altered dry
583 season length and plant inputs on soluble soil carbon, *Ecology*, 99, 2348-2362, <https://doi.org/10.1002/ecy.2473>, 2018.

584 Hua, Q., Turnbull, J. C., Santos, G. M., Rakowski, A. Z., Ancapichún, S., De Pol-Holz, R., Hammer, S., Lehman, S. J.,
585 Levin, I., Miller, J. B., Palmer, J. G., and Turney, C. S. M.: ATMOSPHERIC RADIOCARBON FOR THE PERIOD 1950–
586 2019, *Radiocarbon*, 64, 723-745, [10.1017/RDC.2021.95](https://doi.org/10.1017/RDC.2021.95), 2022.

587 Huang, Y., Bol, R., Harkness, D. D., Ineson, P., and Eglinton, G.: Post-glacial variations in distributions, ¹³C and ¹⁴C
588 contents of aliphatic hydrocarbons and bulk organic matter in three types of British acid upland soils, *Organic Geochemistry*,
589 24, 273-287, [http://dx.doi.org/10.1016/0146-6380\(96\)00039-3](https://doi.org/10.1016/0146-6380(96)00039-3), 1996.

- 590 Hwang, J. and Druffel, E. R. M.: Lipid-Like Material as the Source of the Uncharacterized Organic Carbon in the Ocean?,
591 Science, 299, 881-884, doi:10.1126/science.1078508, 2003.
- 592 Ishikawa, N. F., Itahashi, Y., Blattmann, T. M., Takano, Y., Ogawa, N. O., Yamane, M., Yokoyama, Y., Nagata, T., Yoneda,
593 M., Haghypour, N., Eglinton, T. I., and Ohkouchi, N.: Improved Method for Isolation and Purification of Underivatized
594 Amino Acids for Radiocarbon Analysis, Analytical Chemistry, 90, 12035-12041, 10.1021/acs.analchem.8b02693, 2018.
- 595 Jia, J., Liu, Z., Haghypour, N., Wacker, L., Zhang, H., Sierra, C. A., Ma, T., Wang, Y., Chen, L., Luo, A., Wang, Z., He, J.-
596 S., Zhao, M., Eglinton, T. I., and Feng, X.: Molecular ¹⁴C evidence for contrasting turnover and temperature sensitivity of
597 soil organic matter components, Ecology Letters, 26, 778-788, <https://doi.org/10.1111/ele.14204>, 2023.
- 598 Jobbágy, E. G. and Jackson, R. B.: THE VERTICAL DISTRIBUTION OF SOIL ORGANIC CARBON AND ITS
599 RELATION TO CLIMATE AND VEGETATION, Ecological Applications, 10, 423-436, [https://doi.org/10.1890/1051-0761\(2000\)010\[0423:TVDOSO\]2.0.CO;2](https://doi.org/10.1890/1051-0761(2000)010[0423:TVDOSO]2.0.CO;2), 2000.
- 601 Keiluweit, M., Bougoure, J. J., Nico, P. S., Pett-Ridge, J., Weber, P. K., and Kleber, M.: Mineral protection of soil carbon
602 counteracted by root exudates, Nature Climate Change, 5, 588-595, 2015.
- 603 Kleber, M., Sollins, P., and Sutton, R.: A conceptual model of organo-mineral interactions in soils: self-assembly of organic
604 molecular fragments into zonal structures on mineral surfaces, Biogeochemistry, 85, 9-24, 2007.
- 605 Kleber, M. et al., 2021. Dynamic interactions at the mineral–organic matter interface. Nature Reviews Earth & Environment,
606 2(6): 402-421.
- 607 Kögel-Knabner, I.: The macromolecular organic composition of plant and microbial residues as inputs to soil organic matter,
608 Soil Biology and Biochemistry, 34, 139-162, [https://doi.org/10.1016/S0038-0717\(01\)00158-4](https://doi.org/10.1016/S0038-0717(01)00158-4), 2002.
- 609 Kotanen, P. M.: Revegetation following Soil Disturbance and Invasion in a Californian Meadow: a 10-year History of
610 Recovery, Biological Invasions, 6, 245-254, 10.1023/B:BINV.0000022145.03215.4f, 2004.
- 611 Kuzyakov, Y., Bogomolova, I., and Glaser, B.: Biochar stability in soil: Decomposition during eight years and
612 transformation as assessed by compound-specific ¹⁴C analysis, Soil Biology and Biochemistry, 70, 229-236,
613 <http://dx.doi.org/10.1016/j.soilbio.2013.12.021>, 2014.
- 614 Lavalley, J. M., Soong, J. L., and Cotrufo, M. F.: Conceptualizing soil organic matter into particulate and mineral-associated
615 forms to address global change in the 21st century, Global Change Biology, 26, 261-273, <https://doi.org/10.1111/gcb.14859>,
616 2020.
- 617 Lechleitner, F. A., Baldini, J. U. L., Breitenbach, S. F. M., Fohlmeister, J., McIntyre, C., Goswami, B., Jamieson, R. A., van
618 der Voort, T. S., Prufer, K., Marwan, N., Culleton, B. J., Kennett, D. J., Asmerom, Y., Polyak, V., and Eglinton, T. I.:
619 Hydrological and climatological controls on radiocarbon concentrations in a tropical stalagmite, Geochimica et
620 Cosmochimica Acta, 194, 233-252, <https://doi.org/10.1016/j.gca.2016.08.039>, 2016.
- 621 Lehmann, J. and Kleber, M.: The contentious nature of soil organic matter, Nature, 528, 60-68, 10.1038/nature16069, 2015.
- 622 Lehmann, J., Hansel, C. M., Kaiser, C., Kleber, M., Maher, K., Manzoni, S., Nunan, N., Reichstein, M., Schimel, J. P., Torn,
623 M. S., Wieder, W. R., and Kögel-Knabner, I.: Persistence of soil organic carbon caused by functional complexity, Nature
624 Geoscience, 13, 529-534, 10.1038/s41561-020-0612-3, 2020.

- 625 Levin, I., Heshshaimer, V., 2000. Radiocarbon – A Unique Tracer of Global Carbon Cycle Dynamics. *Radiocarbon*, 42(1):
626 69-80.
- 627 Loh, A. N., Bauer, J. E., and Druffel, E. R. M.: Variable ageing and storage of dissolved organic components in the open
628 ocean, *Nature*, 430, 877-881, 10.1038/nature02780, 2004.
- 629 Lützow, M. v., Kögel-Knabner, I., Ekschmitt, K., Matzner, E., Guggenberger, G., Marschner, B., and Flessa, H.:
630 Stabilization of organic matter in temperate soils: mechanisms and their relevance under different soil conditions - a review,
631 *European Journal of Soil Science*, 57, 426-445, 10.1111/j.1365-2389.2006.00809.x, 2006.
- 632 Marin-Spiotta, E., Chadwick, O. A., Kramer, M., and Carbone, M. S.: Carbon delivery to deep mineral horizons in Hawaiian
633 rain forest soils, *Journal of Geophysical Research: Biogeosciences*, 116, 2011.
- 634 McFarlane, K. J., Torn, M. S., Hanson, P. J., Porras, R. C., Swanston, C. W., Callahan, M. A., and Guilderson, T. P.:
635 Comparison of soil organic matter dynamics at five temperate deciduous forests with physical fractionation and radiocarbon
636 measurements, *Biogeochemistry*, 112, 457-476, 10.1007/s10533-012-9740-1, 2013.
- 637 Mikutta, R., Mikutta, C., Kalbitz, K., Scheel, T., Kaiser, K., and Jahn, R.: Biodegradation of forest floor organic matter
638 bound to minerals via different binding mechanisms, *Geochimica et Cosmochimica Acta*, 71, 2569-2590, 2007.
- 639 Moe, L. A.: Amino acids in the rhizosphere: From plants to microbes, *American Journal of Botany*, 100, 1692-1705,
640 <https://doi.org/10.3732/ajb.1300033>, 2013.
- 641 Nuccio, E. E., Anderson-Furgeson, J., Estera, K. Y., Pett-Ridge, J., De Valpine, P., Brodie, E. L., and Firestone, M. K.:
642 Climate and edaphic controllers influence rhizosphere community assembly for a wild annual grass, *Ecology*, 97, 1307-
643 1318, 10.1890/15-0882.1, 2016.
- 644 Poeplau, C., Don, A., Six, J., Kaiser, M., Benbi, D., Chenu, C., Cotrufo, M. F., Derrien, D., Gioacchini, P., Grand, S.,
645 Gregorich, E., Griepentrog, M., Gunina, A., Haddix, M., Kuzyakov, Y., Kühnel, A., Macdonald, L. M., Soong, J., Trigalet,
646 S., Vermeire, M.-L., Rovira, P., van Wesemael, B., Wiesmeier, M., Yeasmin, S., Yevdokimov, I., and Nieder, R.: Isolating
647 organic carbon fractions with varying turnover rates in temperate agricultural soils – A comprehensive method comparison,
648 *Soil Biology and Biochemistry*, 125, 10-26, <https://doi.org/10.1016/j.soilbio.2018.06.025>, 2018.
- 649 Pries, C. E. H., Ryals, R., Zhu, B., Min, K., Cooper, A., Goldsmith, S., Pett-Ridge, J., Torn, M., and Berhe, A. A.: The Deep
650 Soil Organic Carbon Response to Global Change, *Annual Review of Ecology, Evolution, and Systematics*, 54, 375-401,
651 10.1146/annurev-ecolsys-102320-085332, 2023.
- 652 R Core Team: R: A language and environment for statistical computing., R Foundation for Statistical Computing [code],
653 2019.
- 654 Repasch, M., Scheingross, J. S., Hovius, N., Lupker, M., Wittmann, H., Haghypour, N., Gröcke, D. R., Orfeo, O., Eglinton,
655 T. I., and Sachse, D.: Fluvial organic carbon cycling regulated by sediment transit time and mineral protection, *Nature*
656 *Geoscience*, 14, 842-848, 10.1038/s41561-021-00845-7, 2021.
- 657 Rethemeyer, J., Kramer, C., Gleixner, G., Wiesenberg, G. L. B., Schwark, L., Andersen, N., Nadeau, M.-J., and Grootes, P.
658 M.: Complexity of Soil Organic Matter: AMS 14C Analysis of Soil Lipid Fractions and Individual Compounds,
659 *Radiocarbon*, 46, 465-473, 10.1017/S0033822200039771, 2004.

- 660 Rocci, K. S., Lavallee, J. M., Stewart, C. E., and Cotrufo, M. F.: Soil organic carbon response to global environmental
661 change depends on its distribution between mineral-associated and particulate organic matter: A meta-analysis, *Science of*
662 *The Total Environment*, 793, 148569, <https://doi.org/10.1016/j.scitotenv.2021.148569>, 2021.
- 663 Schmidt, M. W., Torn, M. S., Abiven, S., Dittmar, T., Guggenberger, G., Janssens, I. A., Kleber, M., Kögel-Knabner, I.,
664 Lehmann, J., and Manning, D. A.: Persistence of soil organic matter as an ecosystem property, *Nature*, 478, 49-56, 2011.
- 665 Shi, Z., Allison, S. D., He, Y., Levine, P. A., Hoyt, A. M., Beem-Miller, J., Zhu, Q., Wieder, W. R., Trumbore, S., and
666 Randerson, J. T.: The age distribution of global soil carbon inferred from radiocarbon measurements, *Nature Geoscience*, 13,
667 555-559, 2020.
- 668 Sierra, C. A., Müller, M., and Trumbore, S. E.: Modeling radiocarbon dynamics in soils: SoilR version 1.1, *Geoscientific*
669 *Model Development*, 7, 1919-1931, [10.5194/gmd-7-1919-2014](https://doi.org/10.5194/gmd-7-1919-2014), 2014.
- 670 Silveira, M. L., Comerford, N. B., Reddy, K. R., Cooper, W. T., and El-Rifai, H.: Characterization of soil organic carbon
671 pools by acid hydrolysis, *Geoderma*, 144, 405-414, <https://doi.org/10.1016/j.geoderma.2008.01.002>, 2008.
- 672 Smittenberg, R.H., Eglinton, T.I., Schouten, S., Damsté, J.S.S., 2006. Ongoing Buildup of Refractory Organic Carbon in
673 Boreal Soils During the Holocene. *Science*, 314(5803): 1283-1286.
- 674 Stoner, S., Trumbore, S. E., González-Pérez, J. A., Schrumpf, M., Sierra, C. A., Hoyt, A. M., Chadwick, O., and Doetterl, S.:
675 Relating mineral–organic matter stabilization mechanisms to carbon quality and age distributions using ramped thermal
676 analysis, *Philosophical Transactions of the Royal Society A: Mathematical, Physical and Engineering Sciences*, 381,
677 20230139, [doi:10.1098/rsta.2023.0139](https://doi.org/10.1098/rsta.2023.0139), 2023.
- 678 Stuiver, M. and Polach, H. A.: Discussion Reporting of ¹⁴C Data, *Radiocarbon*, 19, 355-363, [10.1017/s0033822200003672](https://doi.org/10.1017/s0033822200003672),
679 1977.
- 680 Swain, D. L., Langenbrunner, B., Neelin, J. D., and Hall, A.: Increasing precipitation volatility in twenty-first-century
681 California, *Nature Climate Change*, 8, 427-433, [10.1038/s41558-018-0140-y](https://doi.org/10.1038/s41558-018-0140-y), 2018.
- 682 Torn, M. S., Swanston, C. W., Castanha, C., and Trumbore, S. E.: Storage and Turnover of Organic Matter in Soil, in:
683 *Biophysico-Chemical Processes Involving Natural Nonliving Organic Matter in Environmental Systems*, edited by: Senesi,
684 N., Xing, B., and Huang, P. M., Wiley-IUPAC series in biophysico-chemical processes in environmental systems, John Wiley
685 & Sons, Inc., Hoboken, New Jersey, 219-272, 2009.
- 686 Trumbore, S.: Age of Soil Organic Matter and Soil Respiration: Radiocarbon Constraints on Belowground C Dynamics,
687 *Ecological Applications - ECOL APPL*, 10, 399-411, [10.2307/2641102](https://doi.org/10.2307/2641102), 2000.
- 688 Trumbore, S. E. and Harden, J. W.: Accumulation and turnover of carbon in organic and mineral soils of the BOREAS
689 northern study area, *Journal of Geophysical Research: Atmospheres*, 102, 28817-28830, [10.1029/97jd02231](https://doi.org/10.1029/97jd02231), 1997.
- 690 Trumbore, S. E. and Zheng, S.: Comparison of Fractionation Methods for Soil Organic Matter ¹⁴C Analysis, *Radiocarbon*,
691 38, 219-229, [10.1017/s0033822200017598](https://doi.org/10.1017/s0033822200017598), 1996.
- 692 Ukalska-Jaruga, A., Smreczak, B., and Klimkowicz-Pawlas, A.: Soil organic matter composition as a factor affecting the
693 accumulation of polycyclic aromatic hydrocarbons, *Journal of Soils and Sediments*, 19, 1890-1900, [10.1007/s11368-018-](https://doi.org/10.1007/s11368-018-2214-x)
694 2214-x, 2019.

695 van der Voort, T. S., Mannu, U., Hagedorn, F., McIntyre, C., Walthert, L., Schleppi, P., Haghypour, N., and Eglinton, T. I.:
696 Dynamics of deep soil carbon – insights from 14C time series across a climatic gradient, *Biogeosciences*, 16, 3233-3246,
697 10.5194/bg-16-3233-2019, 2019.

698 van der Voort, T. S., Zell, C. I., Hagedorn, F., Feng, X., McIntyre, C. P., Haghypour, N., Graf Pannatier, E., and Eglinton, T.
699 I.: Diverse Soil Carbon Dynamics Expressed at the Molecular Level, *Geophysical Research Letters*, 44, 11,840-811,850,
700 10.1002/2017gl076188, 2017.

701 Vogel, C., Mueller, C. W., Höschen, C., Buegger, F., Heister, K., Schulz, S., Schloter, M., and Kögel-Knabner, I.:
702 Submicron structures provide preferential spots for carbon and nitrogen sequestration in soils, *Nature Communications*, 5,
703 2014.

704 Vogel, J. S., Southon, J. R., Nelson, D. E., and Brown, T. A.: Performance of catalytically condensed carbon for use in
705 accelerator mass spectrometry, *Nuclear Instruments and Methods in Physics Research Section B: Beam Interactions with*
706 *Materials and Atoms*, 5, 289-293, [https://doi.org/10.1016/0168-583X\(84\)90529-9](https://doi.org/10.1016/0168-583X(84)90529-9), 1984.

707 von Lutzow, M., Kogel-Knabner, I., Ekschmitt, K., Flessa, H., Guggenberger, G., Matzner, E., and Marschner, B.: SOM
708 fractionation methods: Relevance to functional pools and to stabilization mechanisms, *Soil Biology and Biochemistry*, 39,
709 2183-2207, 2007.

710 Wang, X.-C. and Druffel, E. R. M.: Radiocarbon and stable carbon isotope compositions of organic compound classes in
711 sediments from the NE Pacific and Southern Oceans, *Marine Chemistry*, 73, 65-81, [https://doi.org/10.1016/S0304-](https://doi.org/10.1016/S0304-4203(00)00090-6)
712 [4203\(00\)00090-6](https://doi.org/10.1016/S0304-4203(00)00090-6), 2001.

713 Wang, X.-C., Callahan, J., and Chen, R. F.: Variability in radiocarbon ages of biochemical compound classes of high
714 molecular weight dissolved organic matter in estuaries, *Estuarine, Coastal and Shelf Science*, 68, 188-194,
715 10.1016/j.ecss.2006.01.018, 2006.

716 Wang, X.-C., Druffel, E. R. M., Griffin, S., Lee, C., and Kashgarian, M.: Radiocarbon studies of organic compound classes
717 in plankton and sediment of the northeastern Pacific Ocean, *Geochimica et Cosmochimica Acta*, 62, 1365-1378,
718 [https://doi.org/10.1016/S0016-7037\(98\)00074-X](https://doi.org/10.1016/S0016-7037(98)00074-X), 1998.

719

720